


A Real-Time Near-Infrared Fluorescence Imaging Method for the Detection of Oral Cancers in Mice Using an Indocyanine Green–Labeled Podoplanin Antibody

Technology in Cancer Research & Treatment
Volume 17: 1-11
© The Author(s) 2018
Reprints and permission:
sagepub.com/journalsPermissions.nav
DOI: 10.1177/1533033818767936
journals.sagepub.com/home/tct


Akihiro Ito, BA^{1,2}, Mitsuhiro Ohta, DDS^{3,4}, Yukinari Kato, MD, PhD⁵, Shunko Inada, PhD⁶, Toshio Kato, MD⁷, Susumu Nakata, MD, PhD⁸, Yasushi Yatabe, MD, PhD², Mitsuo Goto, DDS³, Norio Kaneda, PhD¹, Kenichi Kurita, DDS³, Hayao Nakanishi, MD, PhD^{2,9}, and Kenji Yoshida, DDS³

Abstract

Podoplanin is distinctively overexpressed in oral squamous cell carcinoma than oral benign neoplasms and plays a crucial role in the pathogenesis and metastasis of oral squamous cell carcinoma but its diagnostic application is quite limited. Here, we report a new near-infrared fluorescence imaging method using an indocyanine green (ICG)–labeled anti-podoplanin antibody and a desktop/a handheld ICG detection device for the visualization of oral squamous cell carcinoma–xenografted tumors in nude mice. Both near-infrared imaging methods using a desktop (in vivo imaging system: IVIS) and a handheld device (photodynamic eye: PDE) successfully detected oral squamous cell carcinoma tumors in nude mice in a podoplanin expression–dependent manner with comparable sensitivity. Of these 2 devices, only near-infrared imaging methods using a handheld device visualized oral squamous cell carcinoma xenografts in mice in real time. Furthermore, near-infrared imaging methods using the handheld device (PDE) could detect smaller podoplanin-positive oral squamous cell carcinoma tumors than a non-near-infrared, autofluorescence-based imaging method. Based on these results, a near-infrared imaging method using an ICG-labeled anti-podoplanin antibody and a handheld detection device (PDE) allows the sensitive, semiquantitative, and real-time imaging of oral squamous cell carcinoma tumors and therefore represents a useful tool for the detection and subsequent monitoring of malignant oral neoplasms in both preclinical and some clinical settings.

Keywords

podoplanin, oral squamous cell carcinoma, near-infrared fluorescence imaging, indocyanine green, NZ-I antibody

¹ Graduate School of Pharmaceutical Sciences, Meijo University, Nagoya, Japan

² Department of Pathology and Molecular Diagnostics, Aichi Cancer Center Central Hospital, Nagoya, Japan

³ The First Department of Oral and Maxillofacial Surgery, School of Dentistry, Aichi-Gakuin University, Nagoya, Japan

⁴ Department of Oral and Maxillofacial Surgery, Daiyukai General Hospital, Ichinomiya, Japan

⁵ Department of Regional Innovation, Tohoku University Graduate School of Medicine, Sendai, Japan

⁶ Information and Communications Headquarters/Graduate School of Information Science, Nagoya University, Nagoya, Japan

⁷ Department of Diagnostic Pathology, Daiyukai General Hospital, Ichinomiya, Japan

⁸ Department of Clinical Oncology, Kyoto Pharmaceutical University, Kyoto, Japan

⁹ Laboratory of Pathology and Clinical Research, Aichi Cancer Center Aichi Hospital, Okazaki, Japan

Corresponding Author:

Hayao Nakanishi, MD, PhD, Laboratory of Pathology and Clinical Research, Aichi Cancer Center Aichi Hospital, Kuriyado, Okazaki, Aichi 444-0011, Japan.
Email: hnakanis@aichi-cc.jp



Abbreviations

EGFR, epidermal growth factor receptor; FDA, Food and Drug Administration; ICG, indocyanine green; IRS, immunoreactive score; PDE, photodynamic eye; mAb, monoclonal antibody; NIR, near-infrared; OSCC, oral squamous cell carcinoma; ROI, region of interest.

Received: September 24, 2017; Revised: December 22, 2017; Accepted: February 16, 2018.

Introduction

Oral cancer is the sixth most common cancer worldwide. Although diagnostic and therapeutic modalities have improved, the prognosis of patients with advanced oral squamous cell carcinoma (OSCC) still remains relatively poor, with 5-year survival rates of approximately 50%.¹ The poor prognosis is mainly due to the lack of early detection of OSCC, the high incidence of metastasis/recurrence after surgery, and the chemoresistance of OSCC.^{2,3} A new optical imaging method capable of sensitively and specifically detecting OSCC must be developed to improve the prognosis of OSCC.⁴

Small-sized OSCC is frequently overlooked by conventional examinations under white light but gross inspection is still a gold standard for the screening and diagnosis of oral neoplasms. Recently, a light-induced tissue autofluorescence-based examination has been introduced to assist in screening for OSCC.⁵ Upon illumination by blue light (436 nm), specific components of fluorophores present in the mucosa, including flavin adenine dinucleotide (FAD) and nicotinamide adenine dinucleotide (NAD) in the cross-linked collagen/elastin fibers, emit low-energy light, which is visualized as an autofluorescence image of the mucosa. Malignant transformation is usually associated with an increase in the epithelial cell density, which reduces the excitation of collagen fibers, leading to a decrease in the blue-green autofluorescence and a darker appearance than the uninvolved mucosa. This convenient and sensitive autofluorescence visual imaging technique is a widely used and safe method approved by the US Food and Drug Administration (FDA), but the differentiation of malignant neoplasms from premalignant or benign lesions still remains to be evaluated.^{6,7}

Alternative imaging methods other than autofluorescence-based imaging include imaging of fluorophores synthesized in tissues after the administration of a precursor drug, such as 5-aminolevulinic acid (5-ALA),⁸ and fluorophores injected as exogenous drugs, such as a fluorescent dye-labeled antibody raised against the target molecule.⁹ The latter method has advantages over the former in terms of fewer toxic side effects, such as photo hypersensitivity disorder, as well as higher specificity, leading to its potential utility for molecular targeting therapy. The selection of target molecules for optical imaging is important for the sensitive, specific, and safe detection of oral SCC. Epidermal growth factor receptor (EGFR) is expressed in ~90% of OSCC, and cetuximab, a chimeric

human mouse EGFR antibody, is FDA-approved for clinical use in patients with OSCC, making it a potential target for molecular imaging previously.¹⁰ Another candidate target molecule for molecular imaging of OSCC is podoplanin. Podoplanin is a transmembrane *O*-glycoprotein that binds to C-type lectin-like receptor 2 and shows several important physiological functions¹¹⁻¹³ and unique expression patterns in several tumors, such as squamous cell carcinomas, testicular tumors, mesothelioma, and brain tumors.¹⁴⁻¹⁷ In OSCC, podoplanin is known to be overexpressed in at least 70% to 80% of cases.¹⁸ Podoplanin expression in OSCC was recently shown to be associated with tumor invasion and lymph node metastasis,¹⁹⁻²¹ and podoplanin also possesses prometastatic activities, such as platelet-aggregating activity.²² Furthermore, podoplanin reportedly serves as a molecular marker of cancer stem cells in OSCC.²³ Therefore, podoplanin represents a potential target molecule for molecular imaging and therapy. As reported previously, an anti-podoplanin antibody might be a potential tool for therapy targeting malignant mesothelioma and malignant brain tumors.²⁴⁻²⁶ To our knowledge, however, molecular imaging techniques that target podoplanin as a fluorescence probe in OSCC have not yet been reported. Indocyanine green (ICG), a near-infrared (NIR) fluorophore that has been approved by the FDA for clinical use as a liver function test, has been widely used for sentinel lymph node navigation surgery and real-time identification of liver cancers.^{27,28} Additionally, ICG has been used to label antibodies for molecular imaging,²⁹ raising the possibility of using an ICG-labeled podoplanin antibody for NIR imaging of OSCC in clinical settings.

In the present study, we developed a real-time NIR imaging method that consists of an ICG-labeled podoplanin antibody and a handheld ICG detection system and compared NIR imaging methods with IVIS detection systems and a non-NIR autofluorescence-based method in xenograft models. The pre-clinical and potential clinical applications of this NIR imaging method using an ICG-labeled anti-podoplanin antibody for detecting premalignant and malignant oral neoplasms are discussed.

Materials and Methods

Reagents

A rat monoclonal antibody (mAb) to human podoplanin (NZ-1) was produced previously by Kato *et al.*²⁶ The NZ-1 antibody

was used for molecular imaging, flow cytometry, and immunohistochemistry in mouse tumors. Mouse mAbs against human podoplanin (D2-40) and human EGFR (PharmDX staining kit; DakoCytomation, Carpinteria, California) were used for immunohistochemical staining of clinical specimens because of clear staining pattern. Rat immunoglobulin G (IgG) was purchased from Beckman Coulter (Fullerton, California).

Patients and Ethics Statement

Patients with fibroma, papilloma, leukoplakia, and OSCC (5-7 patients with each type of lesion) were examined in this study. These patients underwent an operation at the Department of Oral and Maxillofacial Surgery at Daiyukai General Hospital from 2011 to 2015. Tumors were removed with either excisional biopsy or partial glossectomy without neck dissection. The tumor stage and histology of OSCC were stage 1 and moderately differentiated SCC, based on the UICC criteria. The use of resected specimens from patients was approved by the Human Ethical Review Committee of the Daiyukai General Hospital, and written informed consent was provided by each participant, with the approval of the institutional review board.

Cell Lines

HSC-3 and Ca9-22 cells were obtained from the RIKEN CELL BANK (Tsukuba, Japan). UMSSC-81 cells were kindly provided by the University of Michigan. These cells were cultured in Dulbecco's Modified Eagle's Medium (Nissui Pharmaceutical Company, Tokyo, Japan) supplemented with 10% fetal bovine serum (Gibco, Grand Island, New York), 100 U/mL of penicillin, and a 100 µg/mL streptomycin solution (Invitrogen Corp, Carlsbad, California) and incubated at 37°C in a 5% CO₂ atmosphere.

Flow Cytometry and Immunofluorescence Staining

Tumor cells were harvested with trypsin/EDTA, washed twice with FACS buffer (5 mM EDTA and 5 mg/mL BSA in PBS) and incubated with a primary rat antihuman podoplanin mAb (NZ-1, 1 µg/mL) for 30 minutes on ice. After washing twice with fluorescence activated cell sorting (FACS) buffer; cells were then incubated with an Alexa Fluor 488-conjugated goat antirat IgG secondary antibody (Invitrogen, Eugene, Oregon) on ice for an additional 30 minutes. The labeled cells were then washed, and the fluorescence intensity was evaluated using a FACS Calibur flow cytometer (BD Biosciences, San Diego, California).

Quantitative Reverse Transcription Polymerase Chain Reaction Analysis

Podoplanin expression was examined by quantitative reverse transcription polymerase chain reaction. Cells were rinsed with PBS and dissolved in ISOGEN (Nippon Gene, Tokyo, Japan).

Total RNA was extracted, and cDNAs were synthesized using SuperScript II RNase H-reverse transcriptase (Invitrogen, Carlsbad, California). Using the resulting first-strand cDNA templates, single-step real-time RT-PCR was performed using the Universal ProbeLibrary system (Roche Diagnostic, Mannheim, Germany), specific oligonucleotide primer pairs, and Taqman probes on the LightCycler instrument. The sequences (5'-3') of the podoplanin primer pairs and Taqman probe number (#) used in this study were described in a previous study.²¹ Glyceraldehyde-3-phosphate dehydrogenase (GAPDH) was analyzed as an internal control. Podoplanin expression in the 3 cell lines was measured in triplicate and compared statistically.

Immunohistochemistry of Paraffin-Embedded Preclinical and Clinical Specimens

Surgically resected tumors from patients (n = 5-7) and xenografts removed from nude mice (n = 3) were fixed with 10% buffered formalin for 24 hours, embedded in paraffin and sectioned to a 5-µm thickness. Immunohistochemical staining of clinical specimens was performed using the following antibodies: a mouse monoclonal antihuman podoplanin mAb (D2-40) and a mouse monoclonal antihuman EGFR mAb (PharmDX staining kit, DakoCytomation, Carpinteria, California) because of clear staining pattern. For antigen retrieval, the sections were microwaved at 98°C for 15 minutes for the D2-40 antibody and treated with a protease K solution for 5 minutes at room temperature for the EGFR antibody. After blocking nonspecific reactions with normal serum for 30 minutes, these sections were incubated with primary antibodies overnight at 4°C, thoroughly washed with PBS, incubated with secondary antibody (biotinylated rabbit antibody to mouse IgG) and subsequently incubated with a streptavidin-peroxidase complex (Vector Laboratories, Burlingame, California) for 60 minutes. For EGFR staining, sections were incubated with secondary antibody labeled by horseradish peroxidase conjugated to a common dextran polymer backbone. The sites of peroxidase binding were visualized using 0.01% diaminobenzidine.

Podoplanin expression was interpreted by visualizing the immunostaining of the specimens and scored using a scoring system based on the quantity and staining intensity of only squamous epithelial tumor cells. The immunoreactive score (IRS; range: 0-15) of each specimen was calculated by multiplying the quantity score (range: 0-5) and staining intensity score (range: 0-3)^{30,31} and was used for the quantitative assessment by statistical analysis (n = 5-7).

Animals

Five- to 6-week-old male athymic nude mice of the KSN strain were purchased from Japan SLC (Hamamatsu, Japan). These mice were housed in specific pathogen-free conditions at Aichi Cancer Center Research Institute. Chlorinated water and food that had been autoclaved for 5 minutes were provided ad libitum. Animal health, including body weight and skin conditions,

was monitored twice weekly. Tumor size was small, with a maximal diameter of 1 cm, and ulceration, a reduction in animal mobility and weight loss, was not observed during the experiment. After imaging experiments, mice were immediately euthanized by cervical dislocation to prevent animals from developing large tumors or weight loss. All experiments were conducted with the approval of the Institutional Ethical Committee for Animal Experiments of Aichi Cancer Center Research Institute (Permission No., ACC 27-2) and met the standards defined by international guidelines.³²

Near-Infrared Imaging of OSCC Xenografts in Mice With an ICG-Labeled Podoplanin Antibody

Three OSCC cell lines (UMSCC-81, HSC-3, and Ca9-22 cells) were harvested with trypsin/EDTA, washed with PBS, and $3\text{--}5 \times 10^6$ cells/0.2 mL PBS were intracutaneously and subcutaneously injected into the upper and lower back, respectively. In some instances, cells (1×10^6 cells/0.05 mL PBS and $3\text{--}5 \times 10^6$ cells/0.3 mL PBS) were injected into the tip of mouse tongue and mouse peritoneal cavity, respectively. For *in vivo* NIR imaging of xenografted tumors in nude mice ($n = 4$), an antipodoplanin antibody (NZ-1; or rat IgG as isotype control) was labeled with ICG using the ICG-Labeling Kit-NH₂ (Dojindo Laboratories, Kumamoto, Japan), according to the manufacturer's protocol.²⁹ In this system, labeling efficiency of ICG to podoplanin antibody (ICG: antibody ratio) was calculated to be average 0.9 (range: 0.8-1.0) based on the following formula: $A_{800}/147,000 \div (A_{280}-A_{800} \times 0.075)/\epsilon$ (= molar absorption coefficient) (A: absorption). In addition, on the stability, this ICG-labeled antipodoplanin antibody was stable at least 1 week and 1 month *in vivo* (in xenograft) and *in vitro*, respectively. Each mouse was intraperitoneally injected with 50 μg of the ICG-labeled podoplanin antibody plus 250 μL of PBS. Indocyanine green fluorescence imaging for intracutaneous, subcutaneous, tongue, and intraperitoneal tumors was performed on mice under isoflurane anesthesia 24 to 48 hours after the injection using an IVIS Lumina II device (Xenogen, Alameda, California) with an excitation filter of 745 nm and the emission filter of approximately 820 nm for ICG. Fluorescence intensity was quantitated as an average radiance (photons/sec/cm²/sr) using "living image" software and the region of interest (ROI) tool, according to the manufacturer's protocol. Alternatively, a handheld ICG imaging device comprising a near-infrared (NIR) light emitting diode (LED) (760 nm, 5 mW/cm²) light source, and ICG camera (830 nm), with high-sensitivity NIR image sensor (768 \times 494 pixel), a photodynamic eye (PDE; Hamamatsu Photonics, Hamamatsu, Japan) was used for the real-time imaging of xenografted tumors in mice ($n = 4$) under 2, 2, 2-tribromethanol anesthesia using the same settings for the exposure time and black balance described in a previous study.²⁷ Fluorescence intensity of the ICG spectrum image of the tumor at 830 nm was quantitated with ImageJ software using ROI after normalization (subtraction) to the background and baseline intensity.

Autofluorescence-Based Imaging of OSCC Xenografts in Mice

Autofluorescence-based imaging of xenografted tumors in nude mice ($n = 3$) under 2, 2, 2-tribromoethanol anesthesia was performed using a VELscope VX device (LED Dental Inc, Burnaby, British Columbia, Canada), which consists of a 120-W metal-halide arc lamp and a filtersystem optimized for producing blue light with 430 (400-460) nm according to the manufacturer's protocol.⁶ Apple green fluorescence images were captured by digital camera with exposure time of 0.1 sec (Sony, Tokyo, Japan).

Statistical Analysis

The statistical significance of differences in RT-PCR data between cell lines was determined by applying Student *t* tests. Differences in ICG fluorescence imaging data between xenograft tumors in nude mice were determined by Mann-whitney *U* test. The difference in the podoplanin expression status based on IRS among benign, premalignant, and malignant neoplasms in patients was analyzed using 1-way analysis of variance. A *P* value $< .05$ was considered significant.

Results

Podoplanin and EGFR Expression in Clinical Specimens of Oral Benign, Premalignant, and Malignant Tumors

Based on the immunohistochemical staining of normal tongue epithelium, podoplanin was weakly expressed and restricted to the basal cell layer of the squamous epithelium. Fibroma in the submucosadid not express podoplanin, with the exception of lymphatic vessels surrounding the tumor. Similarly, podoplanin was weakly expressed in the basal layer of papilloma specimens. In leukoplakia, a premalignant lesion, weak-to-moderate podoplanin expression was observed in the basal cell layer and thin suprabasal layer of the epithelium. In contrast, squamous cell carcinoma exhibited moderate-to-strong podoplanin expression in both basal cells and the thick suprabasal layers (Figure 1A). The quantitative analysis using the IRS scoring system clearly showed that podoplanin expression significantly increased with the grade of pathology in the order of normal (fibroma) $<$ benign (papilloma) $<$ premalignant (leukoplakia) $<$ malignant neoplasm (SCC, $P < .01$; Figure 1C).

On the other hand, EGFR, another potential target for molecular imaging, was expressed at high levels in the basal and upper spinosum layers of normal squamous epithelium and in almost all cell layers of the papilloma and leukoplakia specimens, with the exception of the superficial keratinizing layer, similar to OSCC (Figure 1B). Based on the results of the quantitative analysis, no significant difference in EGFR expression was observed among normal, benign, premalignant, and malignant neoplasms (Figure 1D), indicating that podoplanin is distinctively overexpressed in premalignant and malignant oral neoplasms compared with EGFR.

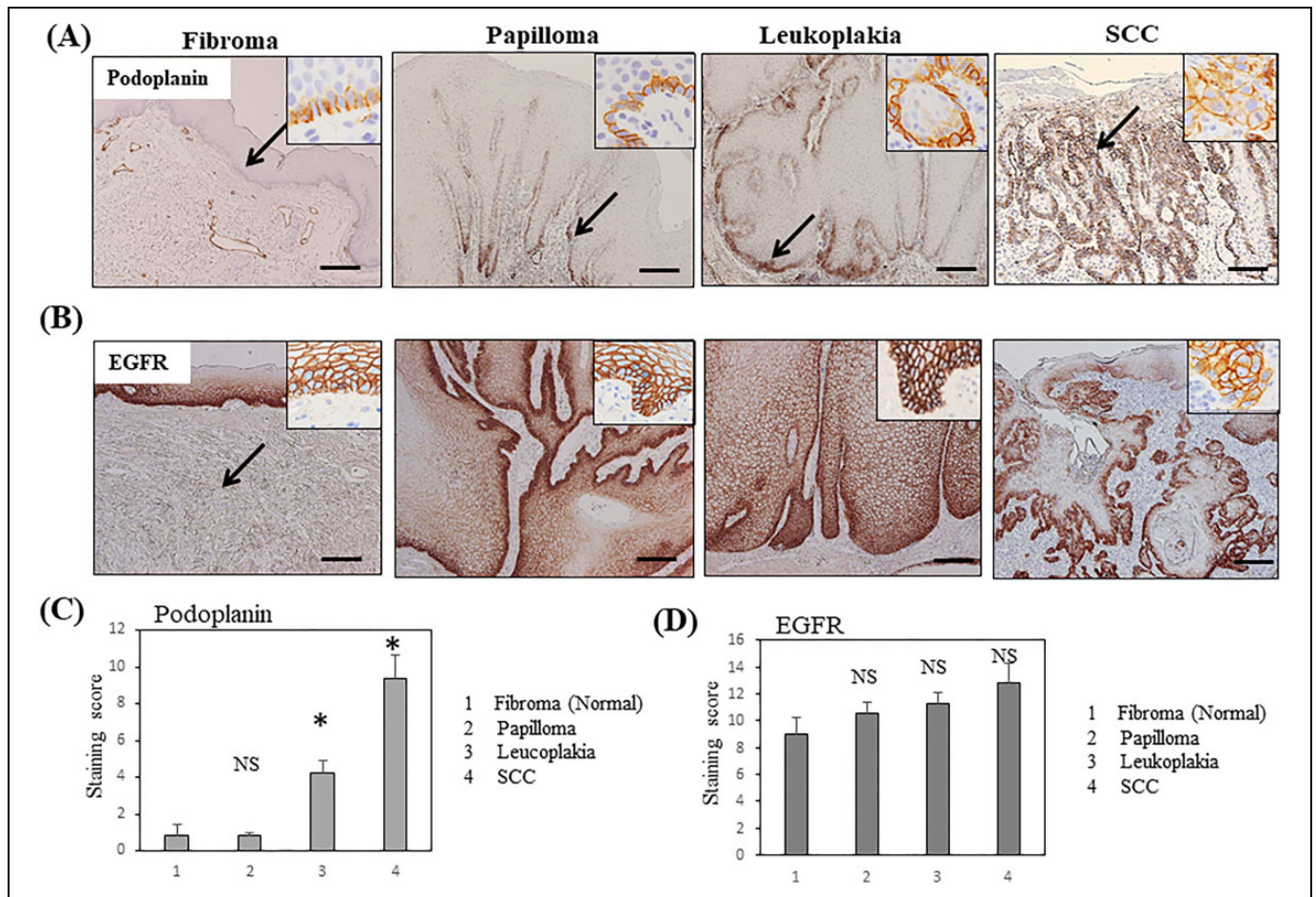


Figure 1. Podoplanin and EGFR expression in clinical specimens from patients with oral neoplasms, as evaluated by immunohistochemistry. A, Podoplanin expression in clinical specimens, including fibroma (normal epithelium), papilloma, leukoplakia, and SCC. Bars = 500 μm. B, EGFR expression in the clinical specimens described above. Insets indicate higher magnification view. C, Quantitative analysis of the intensity of podoplanin staining in normal, papilloma, leukoplakia, and SCC tissues (n = 5-7) based on the immunoreactivity scores. D, Quantitative analysis of the intensity of EGFR staining in normal, papilloma, leukoplakia, and SCC tissues (n = 5-7) based on the immunoreactivity scores. Bar = standard error. * $P < .01$ compared with normal tissues, EGFR indicates epidermal growth factor receptor; NS, not significant; SCC, squamous cell carcinoma.

Podoplanin Expression in OSCC Cell Lines

Podoplanin expression was examined in 3 OSCC cell lines, including UMSCC-81 (poorly differentiated SCC), HSC-3 (moderately differentiated SCC), and Ca9-22 cells (well-differentiated SCC), *in vitro* and *in vivo*. According to the results of the flow cytometry analysis, podoplanin was expressed in these cell lines in the following order: UMSCC-81 > HSC-3 > Ca9-22 cells (Figure 2A). Quantitative RT-PCR analysis of cultured cells confirmed that podoplanin expression was significantly different ($P < .01$) among these cell lines in the following order: UMSCC-81 > HSC-3 > Ca9-22 cells (Figure 2B). An immunohistochemical analysis of xenografted tumor in nude mice showed that podoplanin was expressed at higher levels in these cell lines in the following order: UMSCC-81 > HSC-3 > Ca9-22 cells. UMSCC-81 and HSC-3 cells expressed high and moderate levels of podoplanin in the majority of tumor cells, respectively,

whereas Ca9-22 cells only expressed low levels of podoplanin (Figure 2C).

Near-Infrared Imaging Using an ICG-Labeled Anti-Podoplanin Antibody and an IVIS Detection System

As mentioned above, podoplanin expression was more distinctive for malignant oral neoplasms than EGFR expression. Therefore, in this study, we focused on the utility of an ICG-labeled anti-podoplanin antibody as a probe for NIR fluorescence imaging of OSCC tumors in nude mice. Time-course experiment using intraperitoneal metastasis model of UMSCC-81 cells showed that the labeled antibody accumulated in the intraperitoneal tumors and the unbound residual antibody was first up-taken by the liver and then excreted from the body through intestine in approximately 1-day postinjection of labeled antibody. Near-infrared fluorescence images

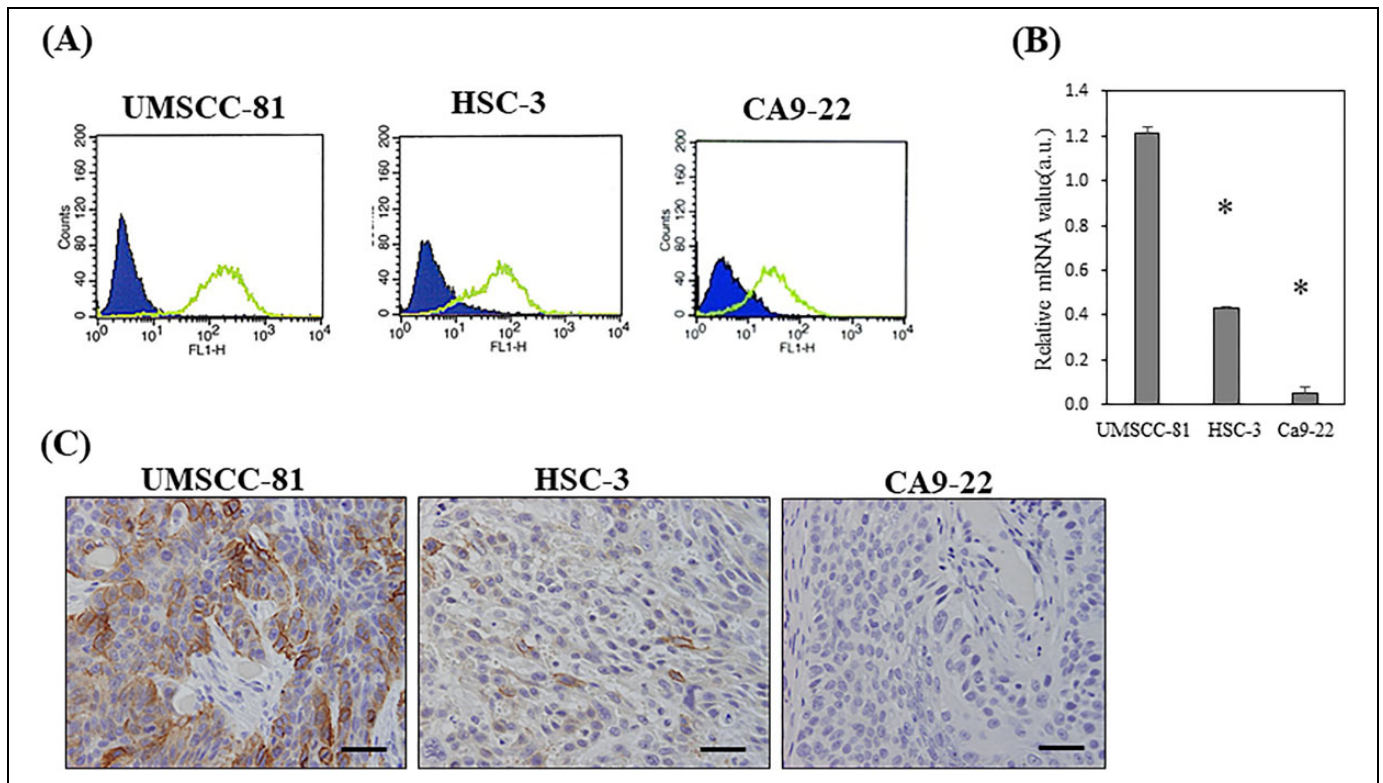


Figure 2. Podoplanin expression in 3 OSCC cell lines *in vitro* and *in vivo*. A, Flow cytometry analysis of 3 OSCC cell lines with different levels of podoplanin expression. Levels of podoplanin expression: UMSCC-81 > HSC-3 > Ca9-22. Blue and green indicates fluorescence staining with isotype control and antipodoplanin antibody, respectively. B, Quantitative RT-PCR analysis of the podoplanin mRNA in 3 OSCC cell lines. $*P < .01$ compared with UMSCC-81 cells. Bar = standard error. C, Immunohistochemical staining of 3 OSCC subcutaneous tumors in nude mice. Strong, moderate, and very weak podoplanin expression was observed in UMSCC-81, HSC-3, and Ca9-22 tumors, respectively. Specimens were counterstained with hematoxylin. Bars = 100 μm . mRNA indicates messenger RNA; OSCC, oral squamous cell carcinoma; RT-PCR, reverse transcriptase polymerase chain reaction.

were available for 1 to 7 days, with the peak fluorescence observed 1 to 3 days after injection (Supplemental Figure A). The NIR fluorescence of intraperitoneal tumor observed using the ICG-labeled antipodoplanin antibody was abolished by the coinjection of an excess amount (10-fold) of unlabeled podoplanin antibody in the blocking experiment (Supplemental Figure B), confirming the specificity of NIR imaging using the ICG-labeled antipodoplanin antibody.

The sensitivity of NIR fluorescent imaging with the ICG-labeled antipodoplanin antibody was then examined using 3 OSCC cell lines with different levels of podoplanin expression. Subcutaneous and tongue tumors generated by UMSCC-81 cells (high expression) and HSC-3 (moderate expression) cells were clearly visible in nude mice using the IVIS imaging system. In contrast, Ca9-22 (very low expression) subcutaneous and tongue tumors were virtually invisible. In addition, no significant fluorescent signal was detected in the SCC xenografts after the intraperitoneal injection of the ICG-labeled rat IgG as a negative control (Figure 3A). The size of xenografted tumors detected with this imaging system was more than 3 mm in diameter. According to the results of the statistical analysis, the ICG fluorescence intensity (photons/sec/cm²/sr) of subcutaneous tumors was increased in the following order: UMSCC-

81 > HSC-3 > Ca9-22 (n = 4 mice each, NS; UMSCC-81 vs HSC-3; $P < .05$, UMSCC-81 vs Ca9-22; Figure 3B). Thus, the ICG fluorescence intensity of tumors in mice was well correlated with the podoplanin expression in tumor cells *in vitro*.

Real-Time NIR Imaging using a Handheld Detection Device (PDE)

We next tested a handheld detection device (PDE) to examine whether PDE detects OSCC tumors in mice in real time after the administration of the ICG-labeled anti-podoplanin antibody (Figure 4A). As shown in the bright and dark field images, PDE can visualize UMSCC-81 and HSC-3 tumors with high-to-moderate podoplanin expression, respectively, in nude mice in real time, but not Ca9-22 tumors with very low podoplanin expression similar to NIR imaging using the ICG-labeled control antibody. Furthermore, PDE detected ICG fluorescence from both intracutaneous tumors and subcutaneous tumors (Figure 4B).

We quantitatively compared the ICG fluorescence intensity of UMSCC-81, HSC-3, and Ca9-22 tumors (n = 4) by PDE detection device and image analysis with ImageJ software (version 1.45) (Figure 5A). Both intracutaneous and subcutaneous tumors were quantitatively detected by PDE in real time, with

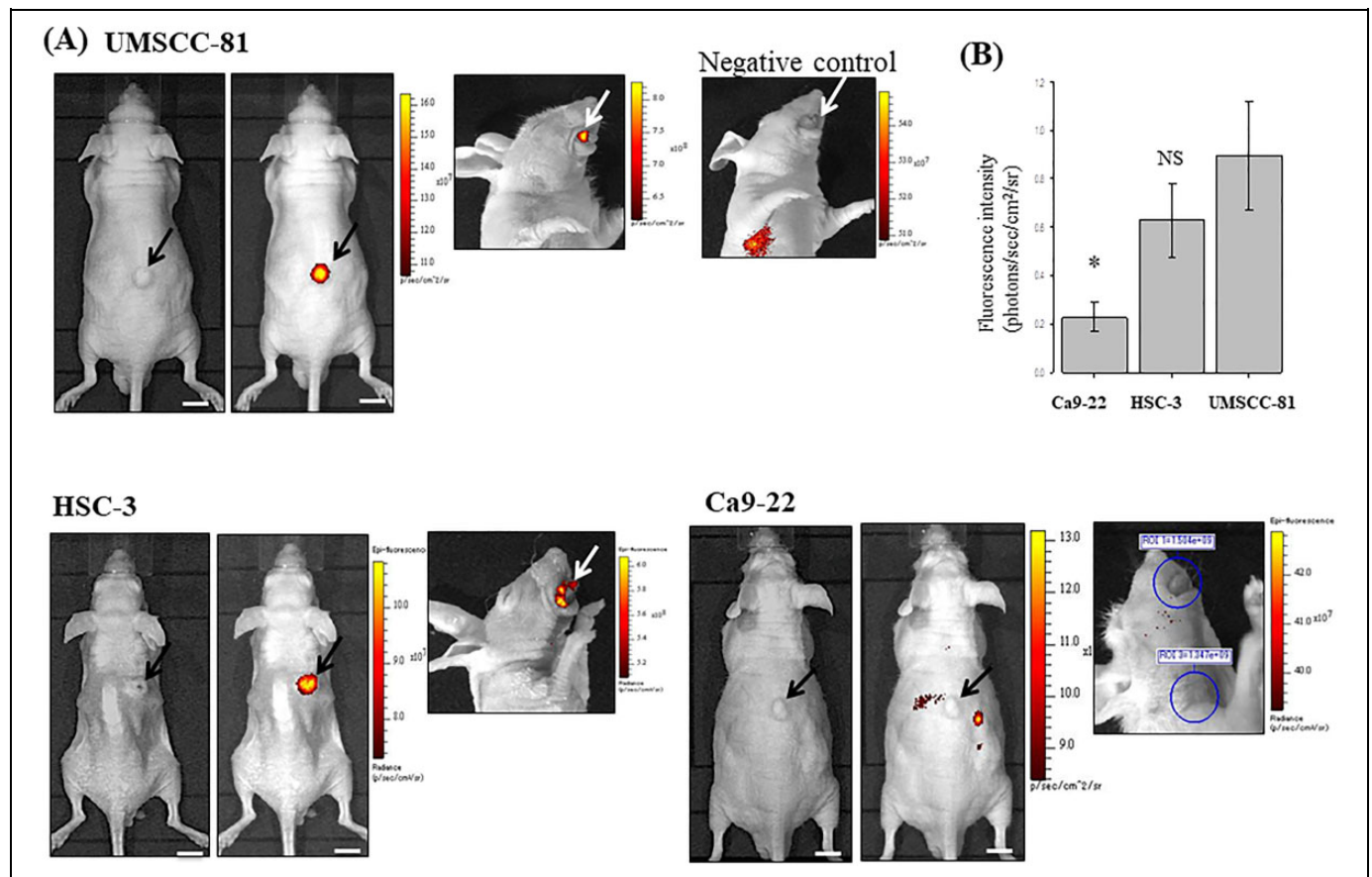


Figure 3. Near-infrared imaging of OSCC xenografted tumors in mice using the ICG-labeled antipodoplanin antibody and IVIS detection device. A, Brightfield (left panel) and dark field images (right panel, pseudocolor image) of subcutaneous tumors (black arrows) and a dark field image of a tongue tumor (white arrows) approximately 1 week after the injection of 3 OSCC cell lines. UMSCC-81 and HSC-3 subcutaneous tumors with high and moderate podoplanin expression, respectively, are clearly visible, whereas Ca9-22 tumors with weak podoplanin expression are virtually invisible. No significant ICG fluorescent signal was observed in the UMSCC-81 tongue tumor using NIR imaging with an ICG-labeled rat IgG as a negative control (upper right panel). B, Quantitative analysis of NIR fluorescent intensity of UMSCC-81, HSC-3, and Ca9-22 subcutaneous tumors in mice ($n = 4$). Bar = standard deviation. * $P < .05$ compared with UMSCC-81 tumors. ICG indicates indocyanine green; IgG, immunoglobulin G; NIR, near-infrared; NS, not significant; OSCC, oral squamous cell carcinoma.

the following order of fluorescence intensity: UMSCC-81 > HSC-3 > Ca9-22 ($n = 4$ mice each, NS; UMSCC-81 vs HSC-3; $P < .05$, UMSCC-81 vs Ca9-22; Figure 5B). These findings are consistent with the podoplanin expression in subcutaneous tumors measured by NIR imaging using the IVIS detection system. Indocyanine green fluorescence at low level in the liver, irrespective of tumor-bearing mice is observed, indicating transient accumulation in the liver as an excretory organ for ICG.

The autofluorescence-based method using the VELscope system also detected both intracutaneous and subcutaneous tumors as “punched-out” lesions, but the latter images are sometimes weaker and less clear than NIR images using the ICG-labeled anti-podoplanin antibody, due to the reduced penetration of blue light for excitation through the skin (Figure 6).

Discussion

In the present study, we developed a real-time NIR imaging method for OSCC using an ICG-labeled anti-podoplanin

antibody in combination with a handheld ICG detection device (PDE). This imaging system has the following advantages over the conventional NIR imaging method using an IVIS detection device and the non-NIR autofluorescence-based imaging method. (1) This system allows positive and clear images of small intracutaneous, subcutaneous, and tongue OSCC tumors with a diameter greater than 3 mm. (2) This system allows the semiquantitative detection of podoplanin-positive OSCC tumors in mice in a podoplanin expression-dependent manner. (3) This system also allows the real-time detection of OSCC tumors compared with imaging methods using the desktop detection device (IVIS). Photodynamic eye is a convenient and small-sized device that fairly comparable to the autofluorescence-based method.^{27,28} These findings suggest that this NIR imaging method using the ICG-podoplanin antibody and a handheld detection device (PDE) would be an useful tool for real-time imaging of OSCC in preclinical and in some clinical studies.

On the other hand, an inherent problem with this imaging system using the ICG-labeled antipodoplanin antibody exists:

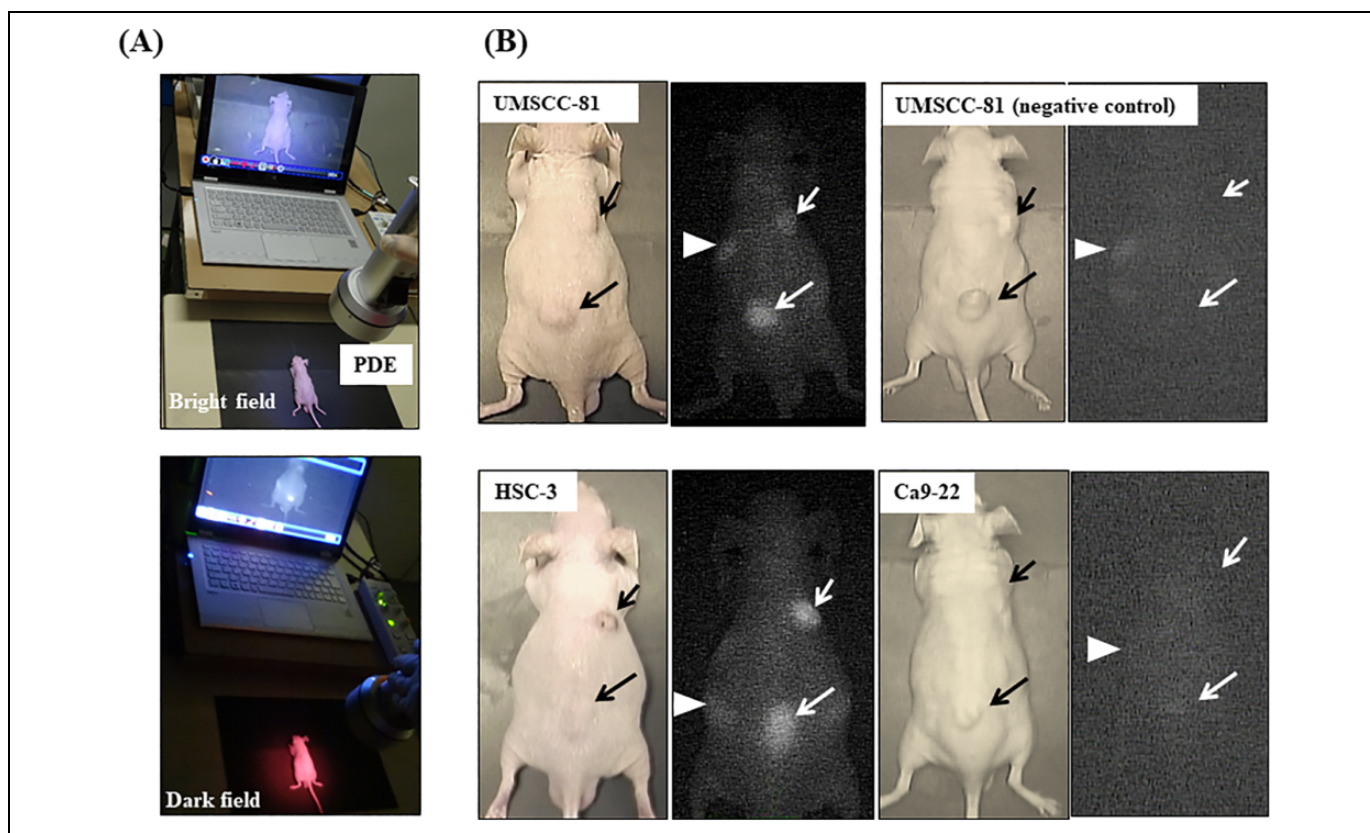


Figure 4. Real-time NIR imaging of OSCC-xenografted tumors in mice using the ICG-labeled anti-podoplanin antibody and a handheld ICG detection device (PDE). A, Overview of real-time NIR imaging using PDE. Bright field (upper panel) and dark field images (lower panel). B, Representative real-time NIR images of UMSCC-81, HSC-3, and Ca9-22-xenografted tumors. No significant ICG fluorescent signal was observed in the UMSCC-81 tumor using the ICG-labeled rat IgG as a negative control (upper right panel). Short arrows and long arrows indicate intracutaneous and subcutaneous tumors, respectively. Arrowheads indicate the liver. ICG indicates indocyanine green; IgG, immunoglobulin G; NIR, near-infrared; OSCC, oral squamous cell carcinoma; PDE, photodynamic eye.

the potential risk of missing 20% to 30% of podoplanin-negative OSCCs and some premalignant lesions. Other disadvantages of this ICG-based imaging system for the detection of OSCC include minimal invasiveness, possible antibody-related side effects, and some cost due to the intravenous injection of the ICG-labeled antibody before imaging compared with the autofluorescence-based method without any requirement for a pretreatment. Furthermore, the safety of NH_2 -reactive ICG for antibody labeling, which includes an active(succinimidyl) ester group in the ICG molecule, remains to be elucidated, although the use of ICG itself has been well established in clinical practice. Unlike computed tomography (CT)/magnetic resonance imaging (MRI)/positron emission tomography (PET), the major limitation of optical imaging, including our NIR imaging system and non-NIR autofluorescence-based method, is the difficulty in applying these technique to the whole-body imaging of tumors located in the deep organs because of the low tissue penetration of the light even if NIR light. However, regarding oral cancer, this is not a limiting factor in clinical settings because of the superficial location of oral tumors.

This NIR imaging method using an ICG-antipodoplanin antibody and a handheld device (PDE) is not only applicable to mouse preclinical models but also applicable to the detection

of podoplanin-positive OSCC in some clinical settings. Several potential clinical applications should be considered. (1) The first application of this ICG imaging method is image-guided surgery, an option for minimizing the risk of residual tumors and resection volume of the healthy tissue by visualizing the tumor margin. (2) The second application of this imaging method is the prediction and monitoring of efficacy of future molecular-targeting therapy using the antipodoplanin antibody.³³ The present finding that the ICG-labeled antipodoplanin antibody efficiently accumulated in OSCC xenografts in mice for a prolonged period (at least 1 week) suggests its potential therapeutic efficacy for OSCC. Podoplanin was recently reported to be a good target for molecular therapy in podoplanin-positive malignant mesothelioma and glioma. As shown in the study by Abe *et al*, the podoplanin antibody (NZ-8/NZ-1) significantly reduces the growth of subcutaneous tumors generated by malignant mesothelioma cells through natural killer (NK) cell-mediated, antibody-dependent cellular cytotoxicity (ADCC).²⁴ Chandramohan *et al* also reported the antitumor effect of a recombinant antipodoplanin (NZ-1) immunotoxin on malignant brain tumors, such as glioblastoma and medulloblastoma.²⁵ Although the antitumor effect of the podoplanin antibody on OSCC remains to be elucidated, these

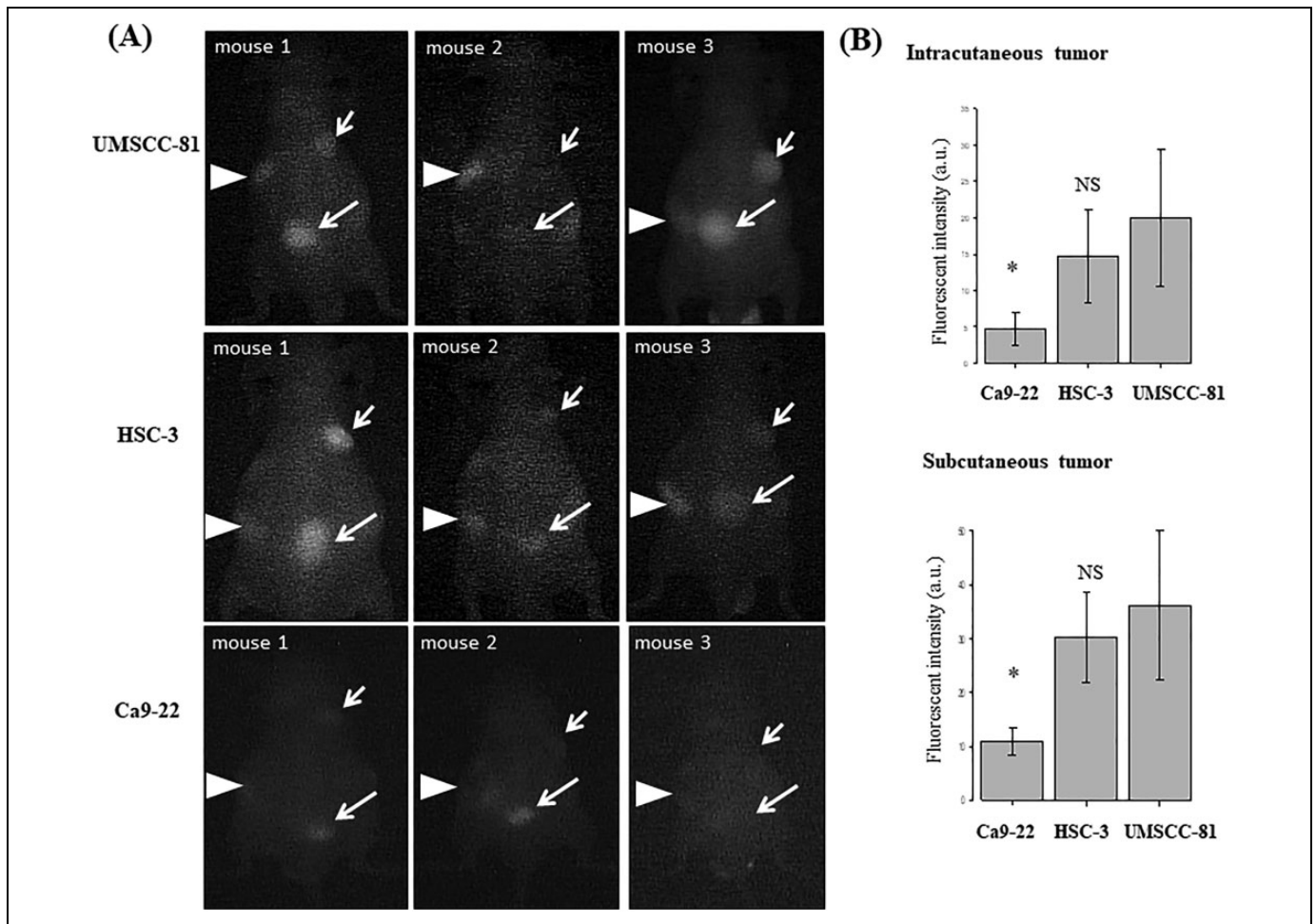


Figure 5. Comparison of real-time NIR images of 3 OSCC-xenografted tumors in mice using the ICG-labeled anti-podoplanin antibody and a handheld detection device (PDE). A, Real-time NIR images (dark field) of 3 OSCC intracutaneous (short arrows) and subcutaneous tumors (long arrows) in mice ($n = 4$). Arrowheads indicate the liver. B, Quantitative analysis of NIR fluorescence intensity of UMSCC-81, HSC-3, and Ca9-22 intracutaneous and subcutaneous tumors. Bar = standard deviation. * $P < .05$ compared with the UMSCC-81 tumors. AU indicates arbitrary units; NIR, near-infrared; NS, not significant; PDE, photodynamic eye; OSCC, oral squamous cell carcinoma.

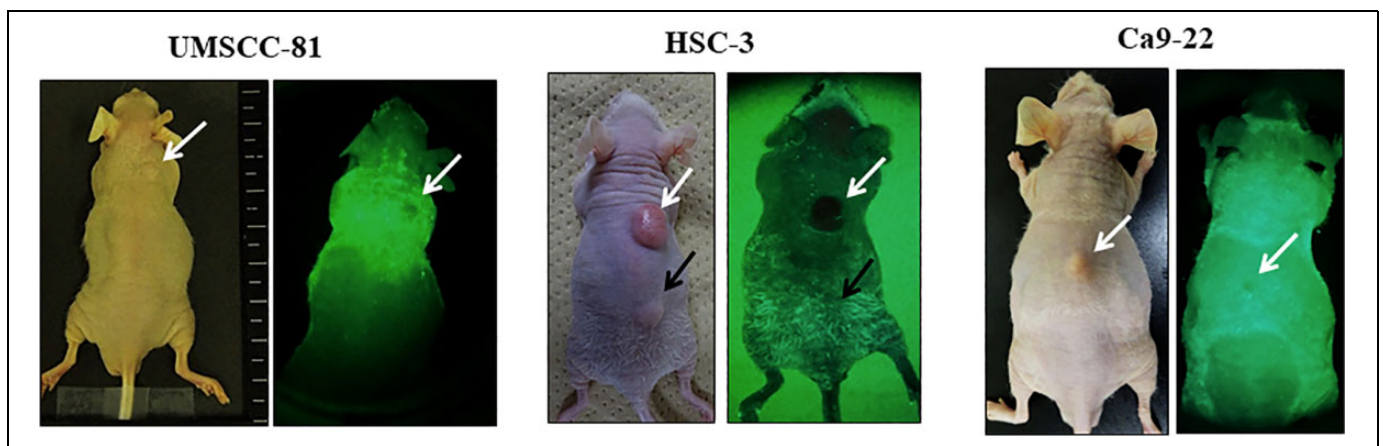


Figure 6. Real-time non-NIR imaging of OSCC-xenografted tumors in mice using the autofluorescence-based method (VELscope). Bright field (left) and dark field (right) images of 3 OSCC intracutaneous (white arrow) and subcutaneous tumors (black arrow in HSC-3 tumors). In the dark field images, UMSCC-81 and HSC-3 intracutaneous tumors (white arrows) are clearly visible as punched-out lesions. Ca9-22 intracutaneous tumors (white arrows) and HSC-3 subcutaneous tumor (black arrow) are only weakly visible. NIR indicates near-infrared; OSCC, oral squamous cell carcinoma.

findings suggest the possibility that real-time NIR imaging with an ICG-labeled antipodoplanin antibody and PDE device may be a useful tool for predicting the sensitivity of molecular targeting therapy using an antipodoplanin antibody in the future clinical settings. (3) The third potential application of this imaging is its utility as an adjunct to the diagnosis of OSCC and premalignant lesions, such as leukoplakia and erythroplakia based on the capability for semiquantitative assessment of podoplanin expression in oral neoplasms. According to de Vicente *et al*, 38% of patients with leukoplakia are classified as podoplanin positive, and the remaining 62% lesions are podoplanin negative.³⁴ Podoplanin expression is significantly correlated with the grade of dysplasia and the risk of progression to OSCC. Similar results were reported in erythroplakia.³⁵ Based on these findings, the semiquantitative evaluation of podoplanin expression using the present ICG imaging method maybe an useful tool to assist the correct diagnosis of premalignant oral lesions and OSCC.

Conclusions

In this study, we developed a new ICG imaging system using an ICG-labeled anti-podoplanin antibody and an ICG detection device (PDE) and showed that this system could clearly visualize OSCC in mice in real time. Although the sensitivity and usability of real-time ICG imaging with a handheld PDE device may be still somewhat insufficient for early diagnosis of OSCC at present, a brighter LED light source, more sensitive/smaller ICG detection camera and a real-time pseudocolor image processor would offer an even greater potential for the real-time diagnosis of OSCC in preclinical and future some clinical settings.

Acknowledgments

The authors would like to thank Ms. M. Yoshimura and N. Saito for their expert technical assistance.

Declaration of Conflicting Interests

The author(s) declared no potential conflicts of interest with respect to the research, authorship and/or publication of this article.

Funding

The author(s) disclosed receipt of the following financial support for the research, authorship, and/or publication of this article: The study was supported by a Grant-in-Aid for Scientific Research from the Ministry of Education, Science, Sports, Culture and Technology (MEXT), Japan, a Grant-in-Aid for Priority Research Project from Knowledge Hub Aichi, Japan and a Grant-in-Aid for the Platform for Drug Discovery, Informatics, and Structural Life Science (PDIS) from Japan Agency for Medical Research and development (AMED), Japan.

Supplemental Material

Supplementary material for this article is available online.

References

- Ong TK, Murphy C, Smith AB, Kanatas AN, Mitchell DA. Survival after surgery for oral cancer: a 30-year experience. *Br J Oral Maxillofac Surg*. 2017;55(9):911-916.
- Bonner JA, Harari PM, Giralt J, et al. Radiotherapy plus cetuximab for locoregionally advanced head and neck cancer: 5-year survival data from a phase 3 randomised trial, and relation between cetuximab-induced rash and survival. *Lancet Oncol*. 2010; 11(1):21-28.
- Naik PP, Das DN, Panda PK, et al. Implications of cancer stem cells in developing therapeutic resistance in oral cancer. *Oral Oncol*. 2016;62:122-135.
- Kossatz S, Weber W, Reiner T. Detection and delineation of oral cancer with a PARP1-targeted optical imaging agent. *Mol Imaging*. 2017;16:1536012117723786.
- Rashid A, Warnakulasuriya S. The use of light-based (optical) detection systems as adjuncts in the detection of oral cancer and oral potentially malignant disorders: a systematic review. *J Oral Pathol Med*. 2003;44(5):307-328.
- Bhatia N, Matias MA, Farah CS. Assessment of a decision making protocol to improve the efficacy of VELscope™ in general dental practice: a prospective evaluation. *Oral Oncol*. 2014; 50(10):1012-1019.
- Warnasukaluriya S. Diagnostic adjuncts on oral cancer and precancer: an update for practitioners. *Br Dent J*. 2017;223(9): 663-666.
- Kitada M, Ohsaki Y, Matsuda Y, Hayashi S, Ishibashi K. Photodynamic diagnosis of pleural malignant lesions with a combination of 5-aminolevulinic acid and intrinsic fluorescence observation systems. *BMC Cancer*. 2015;15(1):174.
- Barrett T, Koyama Y, Hama Y, et al. In vivo diagnosis of epidermal growth factor receptor expression using molecular imaging with a cocktail of optically labeled monoclonal antibodies. *Clin Cancer Res*. 2007;13:6639-6648.
- Day KE, Sweeny L, Kulbersh B, Zinn KR, Rosenthal EL. Pre-clinical comparison of near-infrared-labeled cetuximab and panitumumab for optical imaging of head and neck squamous cell carcinoma. *Mol Imaging Biol*. 2013;15(6):722-729.
- Breiteneder-Geleff S, Matsui K, Soleiman A, et al. Podoplanin, novel 43-kd membrane protein of glomerular epithelial cells, is down-regulated in puromycin nephrosis. *Am J Pathol*. 1997; 151(14):1141-1152.
- Kato Y, Fujita N, Kunita A, et al. Molecular identification of Aggrus/T1alpha as a platelet aggregation-inducing factor expressed in colorectal tumors. *J Biol Chem*. 2003;278(51): 51599-51605.
- Herzog BH, Fu J, Wilson SJ, et al. Podoplanin maintains high endothelial venule integrity by interacting with platelet CLEC-2. *Nature*. 2013;502(7469):105-109.
- Shimada Y, Ishii G, Nagai K, et al. Expression of podoplanin, CD44, and p63 in squamous cell carcinoma of the lung. *Cancer Sci*. 2009;100(11):2054-2059.
- Kahn HJ, Bailey D, Marks A. Monoclonal antibody D2-40, a new marker of lymphatic endothelium, reacts with Kaposi's sarcoma and a subset of angiosarcomas. *Mod Pathol*. 2002;15(4):434-440.
- Kato Y, Sasagawa I, Kaneko M, Osawa M, Fujita N, Tsuruo T. Aggrus: a diagnostic marker that distinguishes seminoma from embryonal carcinoma in testicular germ cell tumors. *Oncogene*. 2004;23(52):8552-8556.

17. Mishima K, Kato Y, Kaneko MK, Nishikawa R, Hirose T, Matsutani M. Increased expression of podoplanin in malignant astrocytic tumors as a novel molecular marker of malignant progression. *Acta Neuropathol.* 2006;111(5):483-488.
18. Yuan P, Temam S, El-Naggar A, et al. Overexpression of podoplanin in oral cancer and its association with poor clinical outcome. *Cancer.* 2006;107(3):563-569.
19. Wicki A, Christofori G. The potential role of podoplanin in tumour invasion. *Br J Cancer.* 2007;96(1):1-5.
20. Huber GF, Fritzsche FR, Züllig L, et al. Podoplanin expression correlates with sentinel lymph node metastasis in early squamous cell carcinomas of the oral cavity and oropharynx. *Int J Cancer.* 2011;129(6):1404-1409.
21. Ohta M, Abe A, Ohno F, et al. Positive and negative regulation of podoplanin expression by TGF- β and histone deacetylase inhibitors in oral and pharyngeal squamous cell carcinoma cell lines. *Oral Oncol.* 2013;49(1):20-26.
22. Toyoshima M, Nakajima M, Yamori T, Tsuruo T. Purification and characterization of the platelet aggregating sialoglycoprotein gp44 expressed by highly metastatic variant cells of mouse colon adenocarcinoma 26. *Cancer Res.* 1995;55(4):767-773.
23. Atsumi N, Ishii G, Kojima M, Sanada M, Fujii S, Ochiai A. Podoplanin, a novel marker of tumor initiating cells in human squamous cell carcinoma A431. *Biochem Biophys Res Commun.* 2008;373(1):36-41.
24. Abe S, Morita Y, Kaneko MK, et al. A novel targeting therapy of malignant mesothelioma using anti-podoplaninantibody. *J Immunol.* 2013;190(12):6239-6249.
25. Chandramohan V, Bao X, Kato Kaneko M, et al. Recombinant anti-podoplanin (NZ-1) immunotoxin for the treatment of malignant brain tumors. *Int J Cancer.* 2013;132(10):2339-2348.
26. Kaneko MK, Kunita A, Abe S, et al. Chimeric anti-podoplanin antibody suppresses tumor metastasis through neutralization and antibody-dependent cellular cytotoxicity. *Cancer Sci.* 2012;103(11):1913-1919.
27. Noura S, Ohue M, Seki Y, et al. Feasibility of a lateral region sentinelnode biopsy of lower rectal cancer guided by indocyanine green using a near-infrared camera system. *Ann Surg Oncol.* 2010;17(1):144-151.
28. Ishizawa T, Fukushima N, Shibahara J, et al. Real-time identification of liver cancers by using indocyanine green fluorescent imaging. *Cancer.* 2009;115(11):2491-2504.
29. Ito A, Ito Y, Matsushima S, et al. New whole-body multimodality imaging of gastric cancer peritoneal metastasis combining fluorescence imaging with ICG-labeled antibody and MRI in mice. *Gastric Cancer.* 2014;17(3):497-507.
30. Rodrigo JP, García-Carracedo D, González MD, Mancebo G, Fresno MF, García-Pedrero J. Podoplanin expression in the development and progression of laryngeal squamous cell carcinomas. *Mol Cancer.* 2010;9:48. doi: 10.1186/1476-4598-9-48.
31. Kawaguchi H, El-Naggar AK, Papadimitrakopoulou V, et al. Podoplanin: a novel marker for oral cancer risk in patients with oral premalignancy. *J Clin Oncol.* 2008;26(3):354-360.
32. Workman P, Aboagye EO, Balkwill F, et al. Committee of the National Cancer Research I. Guidelines for the welfare and use of animals in cancer research. *Br J Cancer.* 2010;102(11):1555-1577.
33. Kato Y, Kaneko MK. A cancer-specific monoclonal antibody recognizes the aberrantly glycosylated podoplanin. *Sci Rep.* 2014;4:5924. doi:10.1038/srep05924.
34. de Vicente JC, Rodrigo JP, Rodriguez-Santamarta T, Lequerica-Fernández P, Allonca E, García-Pedrero JM. Podoplanin expression in oral leukoplakia: tumorigenic role. *Oral Oncol.* 2013;49(6):598-603.
35. Feng JQ, Mi JG, Wu L, et al. Expression of podoplanin and ABCG2 in oral erythroplakia correlate with oral cancer development. *Oral Oncol.* 2012;48(9):848-852.